Solid Freeform Fabrication 2021: Proceedings of the 32nd Annual International Solid Freeform Fabrication Symposium – An Additive Manufacturing Conference
Reviewed Paper

THE LASER POWDER BED FUSION PROCESS DEVELOPMENT OF 17-4 PH STAINLESS STEELS WITH PULSED-WAVE LASERS

Evren Yasa[a*], Andac Ozsoy[b], Erkan Bugra Tureyen[c]

[a]Department of Mechanical Engineering, Eskisehir Osmangazi University, Eskisehir / Turkey
[b]Department of Metallurgical and Materials Engineering, Middle East Technical University, Ankara / Turkey
[c]Department of Mechanical Engineering, Gazi University, Ankara / Turkey

*Corresponding author

Abstract

The main advantage of using Laser Powder Bed Fusion is its unique capability to produce highly complex geometries with intricate features. Besides other differences in powder coating and gas circulation among various LPBF machines, the type of laser (continuous or pulsed wave) is the most critical one. In addition to several process parameters to be optimized for a specific material, pulsed-wave lasers bring extra factors to consider. In this work, a pulsed-wave laser was used to develop process parameters for 17-4 PH stainless steel while keeping volumetric energy density, laser power and velocity constant to understand the effect of pulse related parameters on the outputs. As the point distance (PD) between consecutive laser spots was increased, the exposure time was also raised to keep the scan speed constant. This enabled achieving PDs with one extreme end approaching CW-lasers while the other end aiming at keyhole effect.

Keywords: Pulsed mode, Laser Powder Bed Fusion, point distance, exposure time, 17-4 PH stainless steel

Introduction

Laser Powder Bed Fusion (LPBF) is a powder bed fusion process, which is one of the 7 sub-groups of Additive Manufacturing per ISO/ASTM52900−15 standard [1]. In this process, a 3D object is built in layerwise manner by selectively scanning thin layers of metal powder with an energy of a laser beam as shown in Figure 1. This process utilizes the iterative process of 1) powder deposition 2) laser scanning and solidification 3) moving the build platform downwards until all layers of the part to be built are accomplished. There are many commercial LPBF machines with this concept while employing various powder coating, gas flow, energy source configurations, etc. affecting the part quality and productivity. The laser emission mode is one of the differences although most of the machine vendors prefer a continuous wave (CW) mode laser. Pulsed emission (PW) by power modulation is utilized in a small number of machines due to flexibility in the control over the heat input [2]. This is accomplished by controlling the pulse distance in the scan direction as well as the pulse overlap between consequent scan lines. This flexibility may be beneficial especially for building thin structures such as lattices.

In comparison to CW mode, PW LPBF is less addressed in the literature. The studies conducted to compare CW and PW modes in LPBF are summarized in Table 1. As shown, there are not many studies in the literature comparing PW and CW mode scanning in Laser Powder Bed Fusion. Yet, the results indicate that the emission mode plays a significant role on the outcome. Moreover, in addition to several process parameters to be optimized for a specific

material in LPBF for maximum density, PW mode brings extra factors to consider. In this work, a pulsed-wave laser was employed to develop optimum process parameters for 17-4 PH stainless steel for maximum density while keeping volumetric energy density, laser power and scan speed constant to reveal the influence of pulse related parameters on the outputs such as point distance and exposure time.

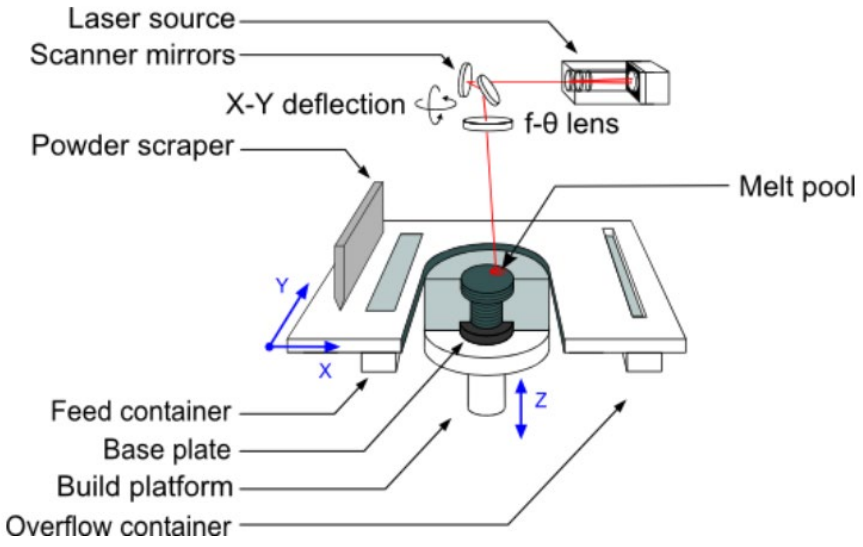

Figure 1 Schematic LPBF Process [3].

Table 1 Comparison Studies of CW and PW mode LPBF processes

Ref.#	Material	Machine	Highlights
[2]	18Ni300 maraging steel	Renishaw AM 250	• Exposure time is critical to improve the part density. • Moving towards CW, porosity is decreased. • PW emission is better for finer geometries.
[4]	AlSi10Mg	Renishaw AM 250 system and LPBF Solutions LPBF 500 system	• Mg_2Si precipitation was observed in CW samples leading to higher hardening. • The macroscopic texture intensity is less pronounced in CW samples due to melt pool geometry.
[5]	AISI 316L stainless steel	In-house developed prototype LPBF system	• Track width and deposited volume is much higher in CW in comparison to PW LPBF. • CW emission leads to a higher melt pool stability in comparison to PW LPBF.
[6]	Ti6Al4V ELI	LPBF 125, Realizer GmbH and LPBF Solutions, 280 HL	• For PW mode, the strut thickness was more uniform in lattice manufacturing whereas CW mode was found more feasible for high density in building larger and denser parts. • CW mode scanning led to a higher level of fatigue life. This is attributed to less number of process-induced imperfections and microstructure.

Methodology

The Test Matrix

In this study, it is aimed to distinguish the effect of pulsed laser parameters from CW laser parameters. Thus, laser power, hatch distance, linear and volumetric energy densities, i.e. LED and VED respectively, were kept constant. As the point distance (PD) between consecutive pulses in the scan direction and exposure time (ET) separates a pulsed laser from a continuous one by replacing the scanning speed, these two parameters were varied in such a way that their ratio PD/ET, i.e. scanning speed, did not change. Doing so, one end of the test matrix was approximated to a CW laser where successive laser shots were fired very closely to each other with low PD and ET values. Laser shots were far separated on the other hand with much higher local energy input to individual spots to keep the VED constant. Although the selected parameters had the same "continuous wave parameters", they were expected to behave differently due to the nature of the PW LPBF. The complete parameter sets are given in Table 2 with corresponding scan speed, LED and VED values.

Table 2 Parameters used in the study.

Index	Power (W)	HD (µm)	PD (µm)	ET (µs)	Scanning Speed (m/s)	LED (J/m)	VED (J/mm^3)
S1	200	110	20	33	0.6	330	100
S2			50	83	0.6	330	100
S3			80	132	0.6	330	100
S4			110	182	0.6	330	100
S5			140	231	0.6	330	100
S6			170	281	0.6	330	100
S7			200	330	0.6	330	100
S8			230	380	0.6	330	100
S9			260	429	0.6	330	100
S10			290	479	0.6	330	100

Experimental Details

The part fabrication was done in a Renishaw AM400 LPBF system equipped with a single pulsed-wave laser with a spot size of 70 µm. The system enables the use of a maximum power output of 400 W. A constant layer thickness of 30 µm was used for all samples. The material subject to investigations was 17-4 PH stainless steel with a particle size distribution of 15-45 µm. The chemical composition of the powders are given in Table 3 below. All builds were done under argon atmosphere with oxygen levels below 500 ppm. The rotating hatch strategy was used with a rotation angle of 67°.

Ten density cubes and ten cylindrical specimens were produced using the parameters given in Table 2. The build scheme is given in Figure 2. The fabricated tensile specimens were in cylindrical form with a nominal diameter of 8 mm. Since the surface roughness of selective laser melted parts is relatively high, perimeter surface of the specimens was machined by turning to the standard diameter of 4 mm according to the ASTM E-8m sub-size cylindrical testing specimen specifications. Tensile testing was carried out at crosshead speed of 1 mm/min using an Instron 5582 Universal Testing Machine equipped with a video extensometer. The tensile axis was parallel to the build direction for all tests and all tests were conducted in as-built condition.

Table 3 Chemical composition of the powders.

Element	Amount (wt.%)	Amount (at.%)
Cr	17.2	18.3
Ni	4.7	4.4
Cu	4.9	4.3
Si	0.4	0.8
Mn	0.5	0.5
Nb	0.4	0.4
C	< 0.07	< 0.32
Fe	Bal.	Bal.

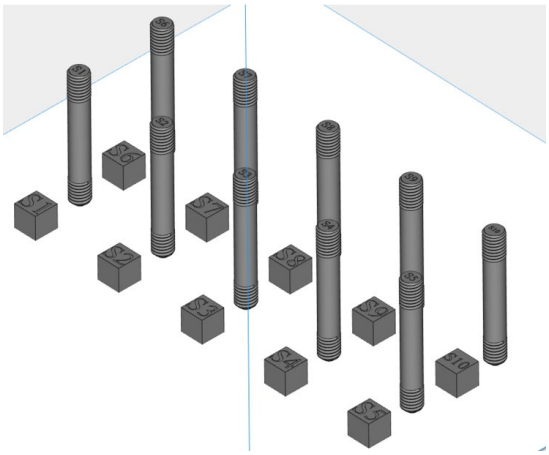

Figure 2 Placement of specimens in the build platform.

The density of the cubes was measured using the Archimedes' method according to ASTM B-311. Before the measurements, a conventionally manufactured 17-4 PH sample was measured to obtain a reference value for the maximum density of 17-4 PH stainless steel, which was measured to be 7.74 g/cm^3. The top and side views of specimens were investigated under an optical microscope and fracture surfaces of the tensile test specimens were studied under SEM. For metallographic investigations, samples were prepared by cutting, grinding and polishing to a surface finish of 1 µm. In order to reveal the grain structure, polished specimens were electro-etched with 10% oxalic acid solution under 15 V for 30 seconds.

Results & Discussion

Densification Behavior

The density results are given in Table 4 together with the parameters used. The relationship between the obtained density versus PD and ET can be seen in Figure 3.

As seen in Figure 3, the relative density sits on a plateau at about 99.5% for most PD-ET combinations. However, after a point distance of 140 µm, individual laser shots are separated so much that the energy given to a point spot fails to compensate for the space in between, creating disrupted scan lines. Moreover, to obtain the same energy density, exposure time has to be increased, which supplies excessive energy to a single point, creating keyhole

porosities characterized by their dome-like shape at the bottom of the meltpools. Keyhole porosities are created due to local excessive energy input, which causes collapsing of the meltpool on itself due to the higher surface tension above [7]. Keyhole porosities are also seen for the low-PD specimens. This can be explained by the inherent differences between PW and CW lasers. As shown by Caprio et al., for a fixed exposure time, total power supplied by the pulsed-laser increases if more shots are requested from the system in a given time, i.e., for an increased duty cycle (see Figure 3 in the reference) [5]. This causes greater energy supplied for reduced point distances than expected as low PD requires successive laser shots in a short period. Moreover, consecutive laser shots that are not sufficiently separated create excessive energy input to assist the formation of keyhole porosities due to heating from the previous laser shots.

Table 4 Relative density results of each parameter set.

Index	Power (W)	HD (µm)	PD (µm)	ET (µs)	Relative Density (%)	Standard Deviation (%)
S1	200	110	20	33	99.37	0.09
S2			50	83	99.74	0.10
S3			80	132	99.41	0.03
S4			110	182	99.52	0.11
S5			140	231	99.54	0.09
S6			170	281	99.36	0.05
S7			200	330	98.84	0.14
S8			230	380	97.77	0.10
S9			260	429	97.44	0.04
S10			290	479	97.61	0.13

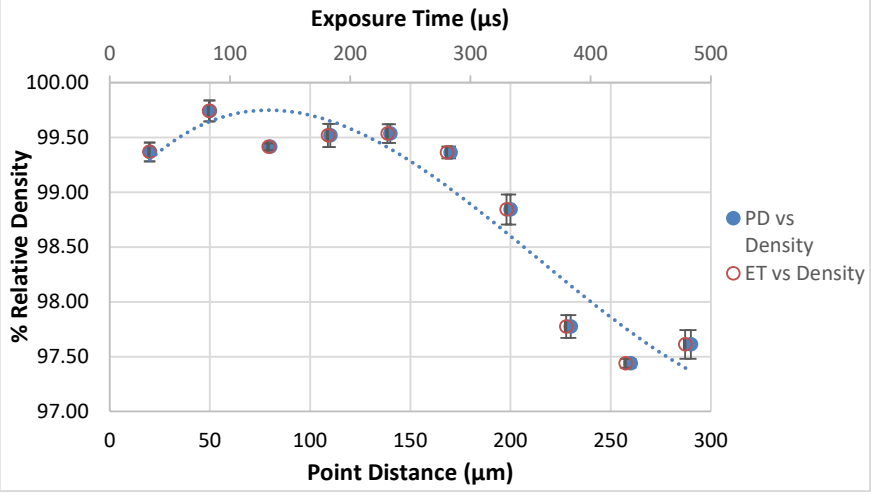

Figure 3 Change in relative density with PD and ET.

Figure 4 shows the energy density distribution of four representative parameters selected among parameters in Table 2. The details for the construction of the graphs are given in [8]. Correspondingly, etched micrographs of these parameters are shown in Figure 5. As shown, the energy distribution for S1 parameter set creates the large keyhole porosities in Figure 5a, due to closely spaced laser shots enlarging the keyhole once it is formed. S3 parameter set creates the most uniform energy distribution, which results in the mostly dense

appearance with only small defects. As PD increases from S3 to S7 and S9, which necessitate ET to increase to keep the same energy density, individual laser shots create the keyhole defects seen in Figure 5c and d. Moreover, it was observed that the continuous laser tracks disappear for S7 and S9 as can be seen from the top views in the same figure.

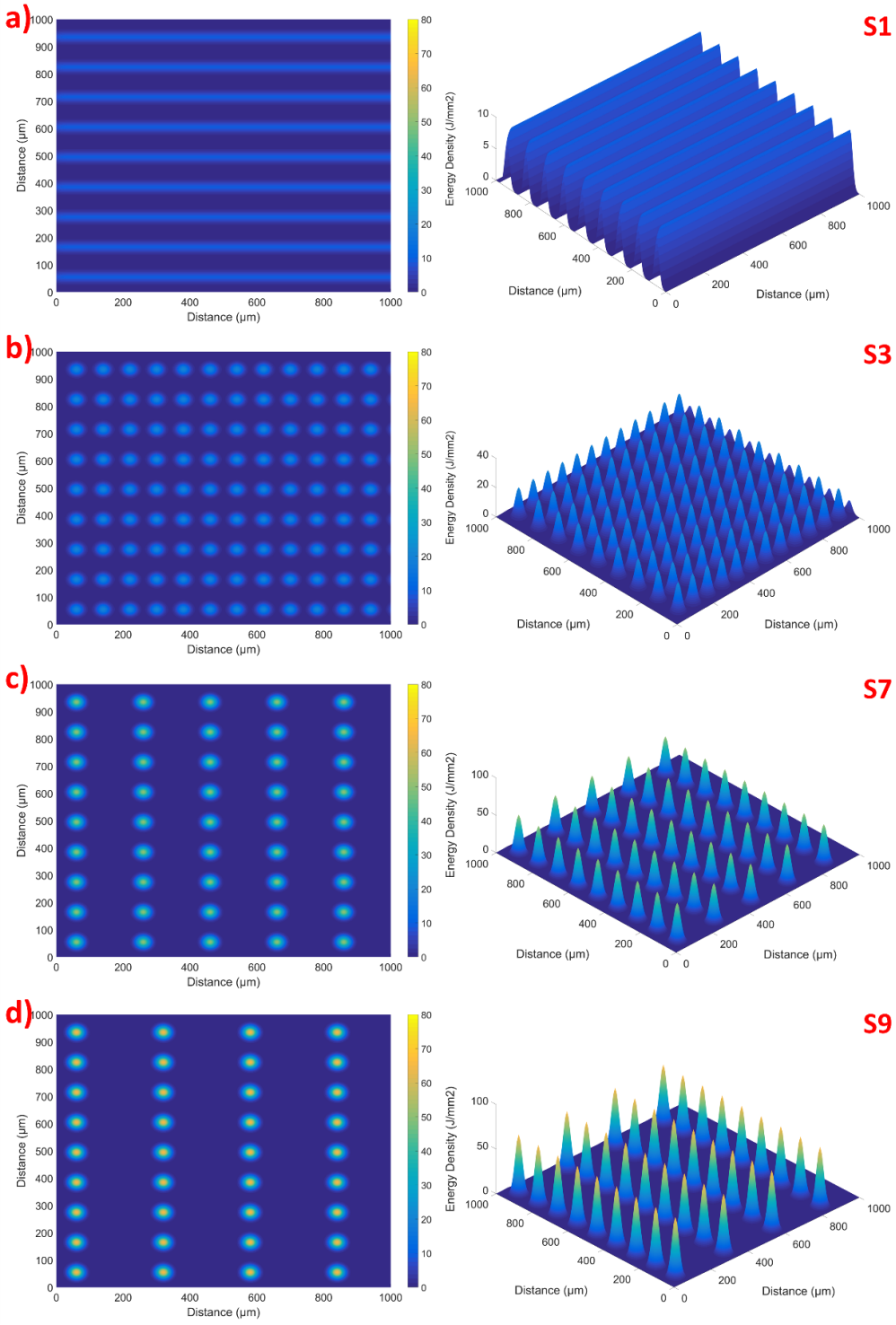

Figure 4 Energy density distribution for parameters a) S1, b) S3, c) S7, d) S9.

These findings show that replacing scanning speed directly by the PD/ET ratio fails in terms of direct applicability. Results that yield acceptable levels of density reside between PD values of 50-140 µm which correspond to point shots overlapped approximately by 33% of the laser spot size and separated by 2 times the spot size, respectively. Although these values may depend on the properties of the material, linear and volumetric energy density which inherently change the melt pool dimensions, this range appears to be a good practice for 17-4 PH stainless steel.

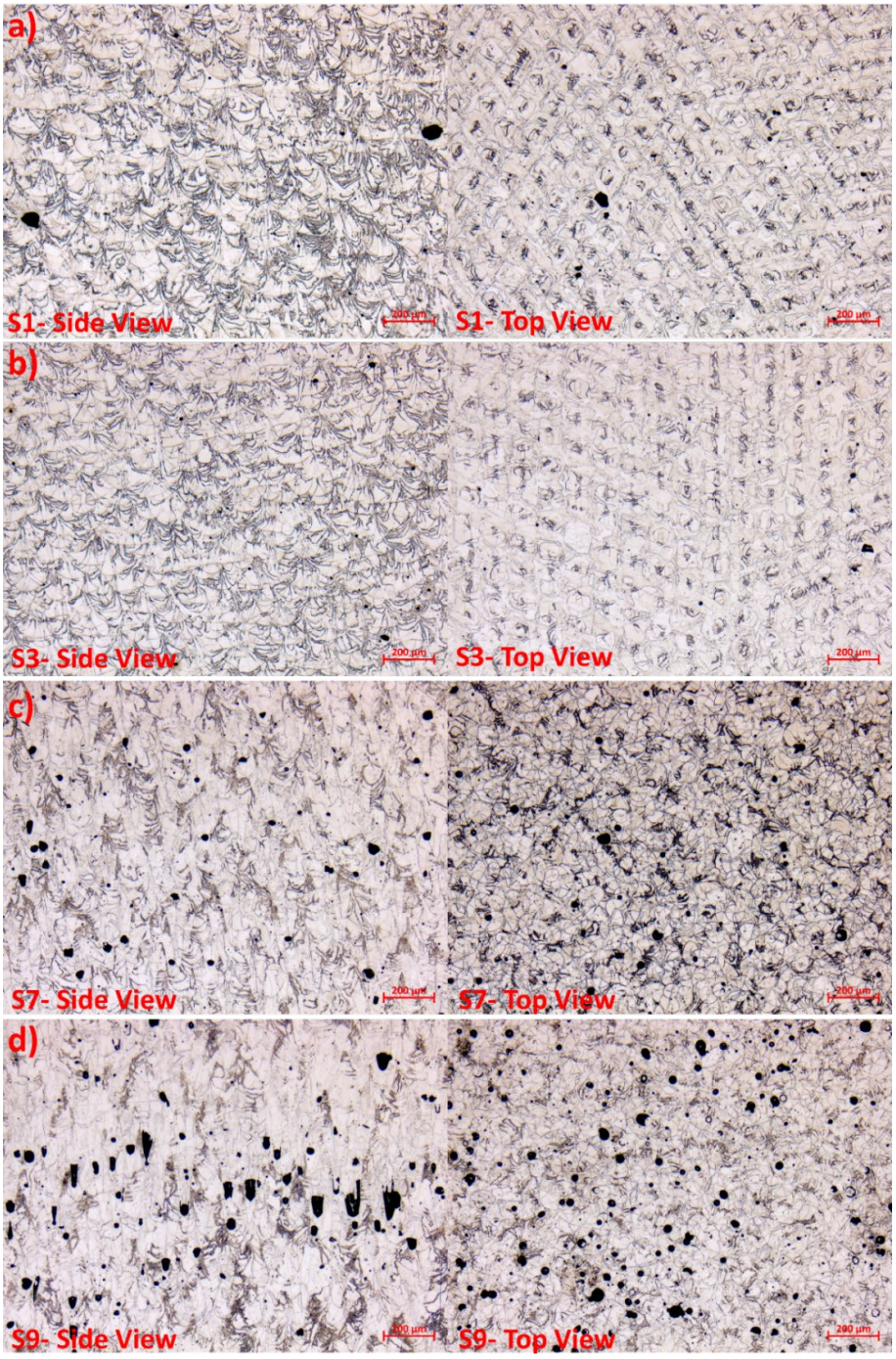

Figure 5 Etched side and top views of specimens fabricated with a) S1, b) S3, c) S7, d) S9 parameter sets.

Tensile Properties

Tensile testing results are given in Figure 6. As depicted, strength values are comparable for the first five parameter sets with elongation values close to 20%. It appears that the large keyhole porosities shown in Figure 5a has little effect on the static tensile properties due to their rounded shape. However, it can be expected that these would be detrimental for dynamic mechanical properties. As the defect density increases for S7, S8, S9 and S10, the ductility drops as much as 73%. On the other hand, tensile and yield strength values increase about 10% for these specimens. Normally, it is expected that both elongation and strength values drop upon the introduction of defects [9–11]. The observed behavior may be explained by the morphology and the orientation of defects with respect to the tensile axis. For example, S8 parameter set creates the keyhole porosities elongated in the build (tensile) direction as shown in Figure 7a. On the other hand, S8 specimen possesses a good inter-layer bonding because of the deep melt pools. It is known that the size and orientation of cracks with respect to the loading direction are important when fracture toughness of a material is considered, where defects that are completely parallel to the loading direction can even be disregarded as they cause negligible stress concentration effect [12]. Therefore, as the size of the keyhole porosities perpendicular to the build direction is quite small, they are thought to create less stress concentration than expected of such large defects. Therefore, it is hypothesized that the superior inter-layer bonding, caused by deeper penetration to the layers below, for the high-PD parameter sets results in increased strength while keyhole defects do not cause catastrophic failure upon loading in Z-direction. However, they do decrease ductility remarkably, because once the stress reaches a critical value, stress concentrating effect of the keyhole defects assists propagation of cracks. This effect can be seen in Figure 7b, where fracture surface of S8 specimen is depicted. As seen in the figure, ductile regions exist between keyhole porosities. However, brittle cleavage planes are seen around the keyhole defects which suggests that deformation in the matrix occur until a critical stress is reached and rapid crack propagation around the keyhole defects takes place. It can be expected that these defects would be extremely detrimental if loaded in transverse direction due to their elongated morphology in the build direction. It should be noted that each parameter set was tested with only 1 tensile specimen to see the general trend and thus the drawn conclusions must carefully be checked with more repetitions.

Conclusions

In this study, the effect of unique parameters of pulsed-wave Laser Powder Bed Fusion was investigated for 17-4 PH stainless steel. It was aimed to understand whether considering the ratio of point distance to exposure time as the replacement of scanning speed in continuous-wave lasers is an applicable practice. It is observed that even if all continuous-wave parameters, i.e. scanning speed, hatch distance and energy density, were kept constant, significant variations may arise with the selection of PD-ET combinations. Both decreasing and increasing point distance over an extent lead to the formation of keyhole porosities due to the excessive local energy input. As a best practice, it is found that individual laser shots should neither overlap more than 33% of the laser spot size, nor should they be separated more than twice of the laser spot size.

Tensile results showed a steady trend for low-PD specimens. As PD was increased, a slight increase in strength and a significant loss in ductility was observed. This has been explained by the morphology of the keyhole defects. It was observed that deformation starts in the matrix upon loading and brittle fracture occurs when a critical stress is reached, causing

rapid crack propagation around the keyhole defects. In conclusion, PD-ET combinations must be selected carefully when working with pulsed-wave Laser Powder Bed Fusion equipment to avoid formation of keyhole defects and to obtain desired mechanical properties.

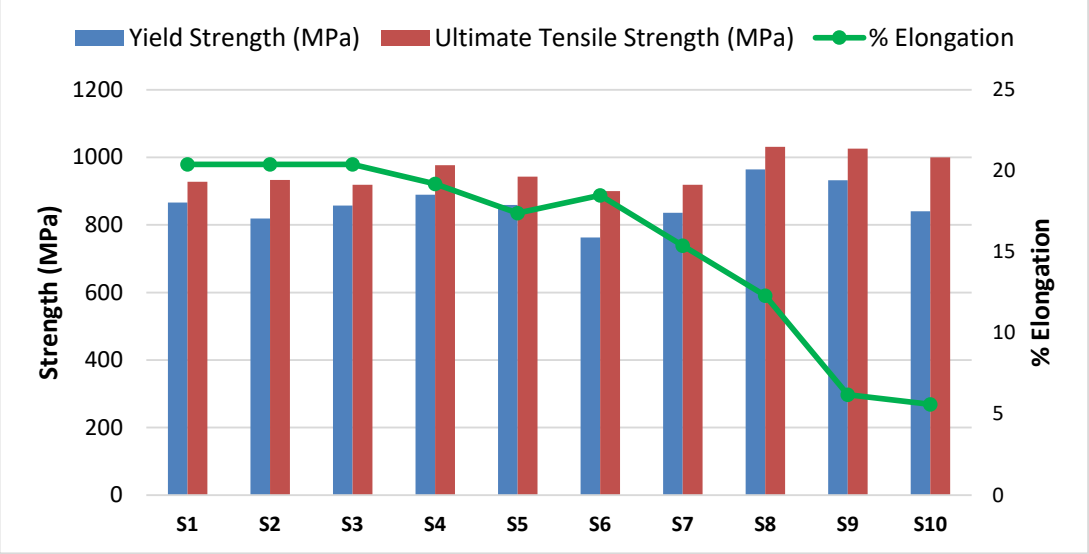

Figure 6 Tensile test results of each parameter set.

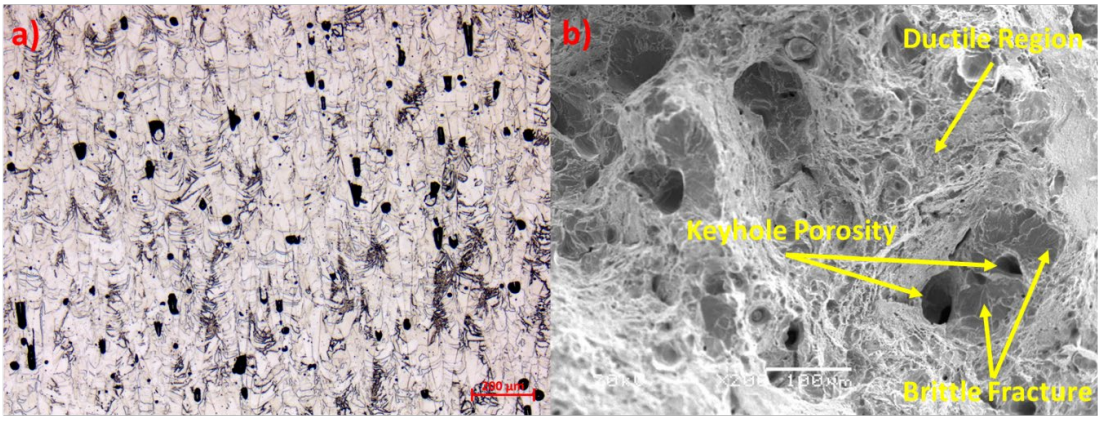

Figure 7 a) Etched side view micrograph and b) fracture surface after tensile test of the specimen fabricated with S8.

References

[1] A. 52900:2015, Standard Terminology for Additive Manufacturing – General Principles – Terminology, ASTM Int. i (2015).

[2] A.G. Demir, P. Colombo, B. Previtali, From pulsed to continuous wave emission in SLM with contemporary fiber laser sources: effect of temporal and spatial pulse overlap in part quality, Int. J. Adv. Manuf. Technol. 91 (2017) 2701–2714. https://doi.org/10.1007/s00170-016-9948-7.

[3] T. Craeghs, S. Clijsters, E. Yasa, J.P. Kruth, Online quality control of selective laser melting, 22nd Annu. Int. Solid Free. Fabr. Symp. - An Addit. Manuf. Conf. SFF 2011. (2011) 212–226.

[4] C.A. Biffi, J. Fiocchi, P. Bassani, A. Tuissi, Continuous wave vs pulsed wave laser emission in selective laser melting of AlSi10Mg parts with industrial optimized process parameters: Microstructure and mechanical behaviour, Addit. Manuf. 24 (2018) 639–646. https://doi.org/10.1016/j.addma.2018.10.021.

[5] L. Caprio, A.G. Demir, B. Previtali, Comparative study between CW and PW emissions in selective laser melting, J. Laser Appl. 30 (2018) 032305. https://doi.org/10.2351/1.5040631.

[6] K. Karami, A. Blok, L. Weber, S.M. Ahmadi, R. Petrov, K. Nikolic, E. V. Borisov, S. Leeflang, C. Ayas, A.A. Zadpoor, M. Mehdipour, E. Reinton, V.A. Popovich, Continuous and pulsed selective laser melting of Ti6Al4V lattice structures: Effect of post-processing on microstructural anisotropy and fatigue behaviour, Addit. Manuf. 36 (2020) 101433. https://doi.org/10.1016/j.addma.2020.101433.

[7] M. Bayat, A. Thanki, S. Mohanty, A. Witvrouw, S. Yang, J. Thorborg, N.S. Tiedje, J.H. Hattel, Keyhole-induced porosities in Laser-based Powder Bed Fusion (L-PBF) of Ti6Al4V: High-fidelity modelling and experimental validation, Addit. Manuf. 30 (2019) 100835. https://doi.org/10.1016/j.addma.2019.100835.

[8] A. Ozsoy, E. Yasa, M. Keles, E.B. Tureyen, Pulsed-mode Selective Laser Melting of 17-4 PH stainless steel: Effect of laser parameters on density and mechanical properties, J. Manuf. Process. 68 (2021) 910–922. https://doi.org/10.1016/j.jmapro.2021.06.017.

[9] H. Gong, K. Rafi, H. Gu, G.D. Janaki Ram, T. Starr, B. Stucker, Influence of defects on mechanical properties of Ti–6Al–4 V components produced by selective laser melting and electron beam melting, Mater. Des. 86 (2015) 545–554. https://doi.org/10.1016/J.MATDES.2015.07.147.

[10] M. Ghayoor, K. Lee, Y. He, C. hung Chang, B.K. Paul, S. Pasebani, Selective laser melting of 304L stainless steel: Role of volumetric energy density on the microstructure, texture and mechanical properties, Addit. Manuf. 32 (2020) 101011. https://doi.org/10.1016/J.ADDMA.2019.101011.

[11] J.H. Yi, J.W. Kang, T.J. Wang, X. Wang, Y.Y. Hu, T. Feng, Y.L. Feng, P.Y. Wu, Effect of laser energy density on the microstructure, mechanical properties, and deformation of Inconel 718 samples fabricated by selective laser melting, J. Alloys Compd. 786 (2019) 481–488. https://doi.org/10.1016/J.JALLCOM.2019.01.377.

[12] J.M. Barsom, S.T. (Stanley T. Rolfe, Fracture and fatigue control in structures : applications of fracture mechanics, ASTM, 1999.